Fluid-present melting of early Archean crust: Stable Sr isotopes from the Kaapvaal Craton

C.-W. Zhang, J.E. Hoffmann, X. Ding, X.-Q. Chen, F. Huang

Supplementary Material

The supplementary material includes:

- Thermodynamic modeling
- The metamorphic overprinting of ~3.45 Ga NG sample
- Rayleigh fractionation modeling
- Binary mixing modeling of mafic and felsic melts
- Discussion: evaluation of potential non-primary factors
- Figures S-1to S-11
- Tables S-1 and S-2
- Supplementary materials references

Thermodynamic modeling

To evaluate the effect of water content and pressure on the crystallization sequence of minerals during magma cooling (rather than modeling the partial melting of a mafic protolith), phase equilibrium modeling was performed for the bulk compositions of sample AGC502T and AGC500 using Perple_X software (version 7.1.9)

(Connolly, 2005) in the MnO-K_2O-Na_2O-CaO-FeO-MgO-Al_2O_3-SiO_2-H_2O-TiO_2-O_2 system with the hp62ver.dat thermodynamic database (Holland and Powell, 2011). Sample AGC502T represents the primitive melt proxy, because it has the lowest SiO_2 (58.67 wt. %) and highest MgO contents, while sample AGC500 represents the evolved end-member (highest SiO_2 content, 69.46 wt. %). Because part of the CaO was hosted in the apatite and P_2O_5 was not included in the modeling due to the lack of phosphorus-bearing mineral activity-solution models, the modeled CaO content was reduced according to the P_2O_5 content in the bulk rock, assuming that all phosphorus is bound to apatite. The following activity-solution models were used: clinopyroxene, melt and amphibole from Green *et al.* (2016); biotite, mica, orthopyroxene, and garnet from White *et al.* (2014); epidote from Holland and Powell (2011); ilmenite from White *et al.* (2000); and feldspar from Holland and Powell (2003). Quartz and titanite are regarded as the pure phase. The $X(Fe^{3+})/\sum(Fe^{2+}+Fe^{3+})$ of the whole rock was fixed at 0.1. The bulk-rock compositions (wt. %) used for phase-equilibrium modeling are summarized in Table S-2.

Two complementary modeling strategies were implemented. For each bulk composition, calculations were first conducted at a fixed pressure of 8 kbar (simulating the mid- to lower-crustal cooling) with temperature ranging from 650 ºC to 1300 ºC and water content of 0–12 wt. % (Fig. S-8). To systematically assess the combined effects of pressure and melt H_2O content on the liquidus temperature of plagioclase and amphibole, P-T pseudosections were performed at 4–10 kbar and 700–1200 ºC, under fixed water content of 2 wt. %, 4 wt. %, and 8 wt. % (Fig. 3). The P-T modeling results in Fig. 3 suggest that, under high melt H_2O conditions (e.g., 8 wt. %), higher pressure depresses the plagioclase liquidus relative to the amphibole liquidus during cooling, indicating that pressure plays a secondary yet supportive role relative to melt H_2O content.

The metamorphic overprinting of ~3.45 Ga NG sample

The NG sample of AGC470 appears to have experienced a complicated metamorphic history. The pyroxene cores were overprinted by amphibole and later biotite. The sample contains abundant late-stage overgrowths of biotite and chlorite, as well as minor amounts of opaque minerals. Collectively, the sample experienced granulite-facies metamorphism followed by retrogression through the amphibolite facies and greenschist facies.

Rayleigh fractionation modeling

To quantify the influence of plagioclase fractionation on stable Sr isotopic composition during magmatic crystallization, Rayleigh fractionation modeling was performed following the approach of Charlier *et al.* (2012):

$$C_{melt} = C_{melt,0} \times F_{melt}^{\,D-1}$$

$$\delta^{88}Sr_{melt} = (\delta^{88}Sr_{melt,\,0} + 1000) \times f_{melt}^{\,\alpha-1} - 1000$$

$$f_{melt} = C_{melt}/C_{melt,0}$$

where C_{melt} and $C_{melt,0}$ denote the Sr concentrations of the residual and initial melts, respectively; D represents the partition coefficient between plagioclase (Pl) and melt; $\delta^{88}Sr_{melt,0}$ and $\delta^{88}Sr_{melt}$ correspond to the stable Sr isotopic compositions of the initial and residual melt, respectively; f_{melt} is the fraction of Sr remaining in the melt; F_{melt} is the residual melt fraction; α is the equilibrium isotope fractionation factor between plagioclase and melt.

The $\alpha_{Pl\text{-}Melt}$ is taken as 1.0007 based on Charlier *et al.* (2012), and alternatively 1.0003, calculated from $\Delta^{88}Sr_{Pl\text{-}Melt} \approx 10^3 ln\alpha_{Pl\text{-}Melt}$ for the Huili granite, China (Chen *et al.*, 2025) in Fig. 2. The partition coefficient *D* (= 4.4) is adopted from Hanson (1978). The mean value of the TG samples $\delta^{88}Sr = 0.25‰$ is used to approximate the initial melt composition. The Sr content of initial melt ($C_{melt,0}$) is assigned a range of 162–393 ppm based on the TG samples (Hoffmann *et al.*, 2016).

Binary mixing modeling of mafic and felsic melts

To evaluate whether the magma mixing hypothesis proposed by Hoffmann *et al.* (2016)—involving mixing between mantle-derived melts and partial melts of the older Ngwane Gneiss (NG)—is applicable to the stable Sr isotope compositions of our samples, we conducted quantitative binary mixing modeling (Fig. S-10). For any mixed product, the fraction of the mafic end-member is denoted as *f* (with $0 \leq f \leq 1$) and that of the felsic end-member as (*1-f*). The concentration of Sr or SiO_2 in the mixture is calculated by:

$$C_{mix} = C_{mafic} \times f + C_{felsic} \times (1-f)$$

where C_{mix}, C_{mafic} and C_{felsic} represent the contents of the relevant component (Sr or SiO_2) in the mixed melt, mafic and felsic end-member. For the stable Sr isotope composition, the composition in the mixed melt is performed by:

$$\delta^{88}Sr_{mix} = (\delta^{88}Sr_{mafic} \times C_{mafic} \times f + \delta^{88}Sr_{felsic} \times C_{felsic} \times (1-f))/C_{mix}$$

where $\delta^{88}Sr_{mix}$, $\delta^{88}Sr_{mafic}$ and $\delta^{88}Sr_{felsic}$ represent the compositions of the mixed melt, mafic and felsic end-member, respectively.

In Fig. S-10a, we modeled binary mixing in Sr concentration versus $\delta^{88}Sr$ space between two end-members: a mantle-derived mafic melt ($\delta^{88}Sr = 0.27‰$) and a felsic melt derived from the NG basement (sample AGC470, $\delta^{88}Sr = 0.10‰$). In Fig. S-10a, four scenarios were tested by varying the Sr concentrations of the end-members: Sr_{mafic} = 25 ppm and 250 ppm, corresponding to the observed range of Sr concentrations in the DSS greenstone belt (~25–250 ppm, Fig. S-7, from Hoffmann *et al.* 2020), and Sr_{felsic} = 161 ppm and 583 ppm, corresponding to the observed range of Sr contents in the TG samples. In Fig. S-10b, binary mixing was evaluated in Sr versus SiO_2 space, using a mafic end-member (SiO_2 = 45 wt. %) and a felsic end-member (SiO_2 = 71 wt. %). Four mixing combinations were calculated using Sr_{mafic} values of 250 ppm and 800 ppm, and Sr_{felsic} values of 161 ppm and 583 ppm. We first used 250 ppm, representing the high-Sr end of the observed range of the DSS mafic rocks. Because this value cannot reproduce the observed Sr-SiO_2 relationships of the TG samples, we additionally tested an extreme high-Sr mafic end-member of 800 ppm to evaluate whether binary mixing could reproduce the observed trend even under an unrealistically high-Sr scenario.

Discussion: evaluation of potential non-primary factors

Weathering and metamorphism

Chemical weathering can fractionate $\delta^{88}Sr$ depending on pH and mineral stability (Luo *et al.*, 2024). However, our samples are remarkably fresh, characterized by low chemical index of alteration (CIA) values (45–51, Table S-1) and low loss on ignition (LOI). The lack of correlation between $\delta^{88}Sr$ and CIA or LOI indicates that subaerial weathering has not significantly modified the primary Sr isotope signatures (Fig. S-5c, S-5d). Similarly, while the TG has undergone metamorphism, the primary reservoirs of Sr (plagioclase, K-feldspar and apatite) remain relatively stable under low- to medium-grade metamorphic conditions. The absence of petrographic evidence for fluid-induced metasomatism, e.g., quartz veining, epidotisation or partial melt veins, suggests that metamorphic overprinting on $\delta^{88}Sr$ is negligible (Hoffmann *et al.*, 2016; Fig. S-11). In addition, the limited variation in $\delta^{88}Sr$, despite variable initial $(^{87}Sr/^{86}Sr)_t$ values (Fig. S-5b), indicates that stable Sr isotope compositions were not substantially modified during post-magmatic processes. The relatively low initial $(^{87}Sr/^{86}Sr)_t$ values of bulk rocks and primary igneous mineral apatite (Davies and Allsopp, 1976; Caton

et al., 2022; this study) further suggest negligible incorporation of older crust and limited post-magmatic disturbance of the Sr isotope system. The heterogeneity in initial $(^{87}Sr/^{86}Sr)_t$ values, however, is interpreted to reflect source heterogeneity rather than metamorphic redistribution, consistent with the heterogeneous whole-rock Hf-Nd isotope compositions (Fig. S-6).

Crustal contamination and magma mixing

The $\delta^{88}Sr$ composition of continental crust exhibits wide variability (Andrews and Jacobson, 2018; Chen *et al.*, 2025). Although the TG intruded the older Ngwane Gneiss (NG) basement, several lines of evidence argue against significant crustal contamination: (i) the TG samples are lithologically homogeneous without field evidence of xenoliths or mixing; (ii) their geochemical signatures deviate from binary mixing between mantle-derived melts and evolved crust (Hoffmann *et al.*, 2016), and (iii) the restricted range of initial $^{87}Sr/^{86}Sr$ ratios supports evolution within a coherent magmatic system.

Regarding magma mixing, while Hoffmann *et al.* (2016) suggested a hybrid origin for the TG, our stable Sr data do not show systematic isotopic shifts expected from the mixing of two distinct end-members. It should be noted that during binary mixing modeling, using the Sr-SiO_2-$\delta^{88}Sr$ compositions of the TG samples to represent the felsic melt end-member is a simplification. The resulting mixing trajectories in Sr-$\delta^{88}Sr$ space fail to capture the observed stable Sr isotope compositions of the TG samples (Fig. S-10a). Although the TG data points align along the Sr-SiO_2 mixing curve corresponding to a mixture between a high-Sr mafic end-member (800 ppm) and a low-Sr felsic end-member (161 ppm), such a high Sr concentration is unlikely for mantle-derived basaltic melts (Fig. S-10b), given that the ~3.46 Ga DSS greenstone belt in the AGC region has Sr content of ~25–250 ppm (Fig. S-7, Hoffmann *et al.*, 2020). The above confirms that magma mixing between mantle-derived melts and partial melts of the older Ngwane Gneiss (NG) cannot explain the petrogenesis of the TG samples.

Furthermore, the decoupling between SiO_2 and $\varepsilon_{Hf}(t)$ and $\varepsilon_{Nd}(t)$ contradicts the high-efficiency mixing model. We suggest that the apparent mixing trends in trace elements reflect source heterogeneity or differentiation paths rather than physical hybridization. Previous mixing models overemphasized plagioclase fractionation (50 wt. % plagioclase and 50 wt. % amphibole) without considering Fe-Ti oxide crystallization, which led to a potential misinterpretation of the liquid line of descent. Fe-Ti oxide crystallization is important

for suppressing Fe-enrichment and driving the residual melt along a calc-alkaline trend (Thy and Lofgren, 1994; Nandedkar *et al*., 2014; Zhang *et al*., 2023).

Partial melting and source residue fingerprinting

During the melting of a mafic source, if plagioclase remains in the residue, it would sequester heavy Sr isotopes, leaving the generated melt (the TG precursor) with a slightly lighter δ^{88}Sr signature (Charlier *et al.*, 2012; Klaver *et al.*, 2020; Chen *et al.*, 2025). However, the TG samples are indistinguishable from the BSE value, which implies that the plagioclase-to-hornblende ratio of the source residue was extremely low. This is consistent with fluid-present melting. Under hydrous conditions, the stability field of plagioclase is drastically reduced while that of hornblende is expanded. The absence of a heavy Sr isotope signature in the melt (which would occur if K-feldspar were the dominant residual phase) (Chen *et al.*, 2025) and the lack of a strong light signature (which would occur with significant plagioclase fractionation) both point to a hornblende-dominated, plagioclase-poor residual assemblage. This provides a new, independent isotope line of evidence for fluid-present melting in the early Archean Kaapvaal crust, as water is the most efficient agent for suppressing plagioclase stability in these settings (Beard and Lofgren, 1991; Pichavant and Macdonald, 2007; Müntener and Ulmer, 2018).

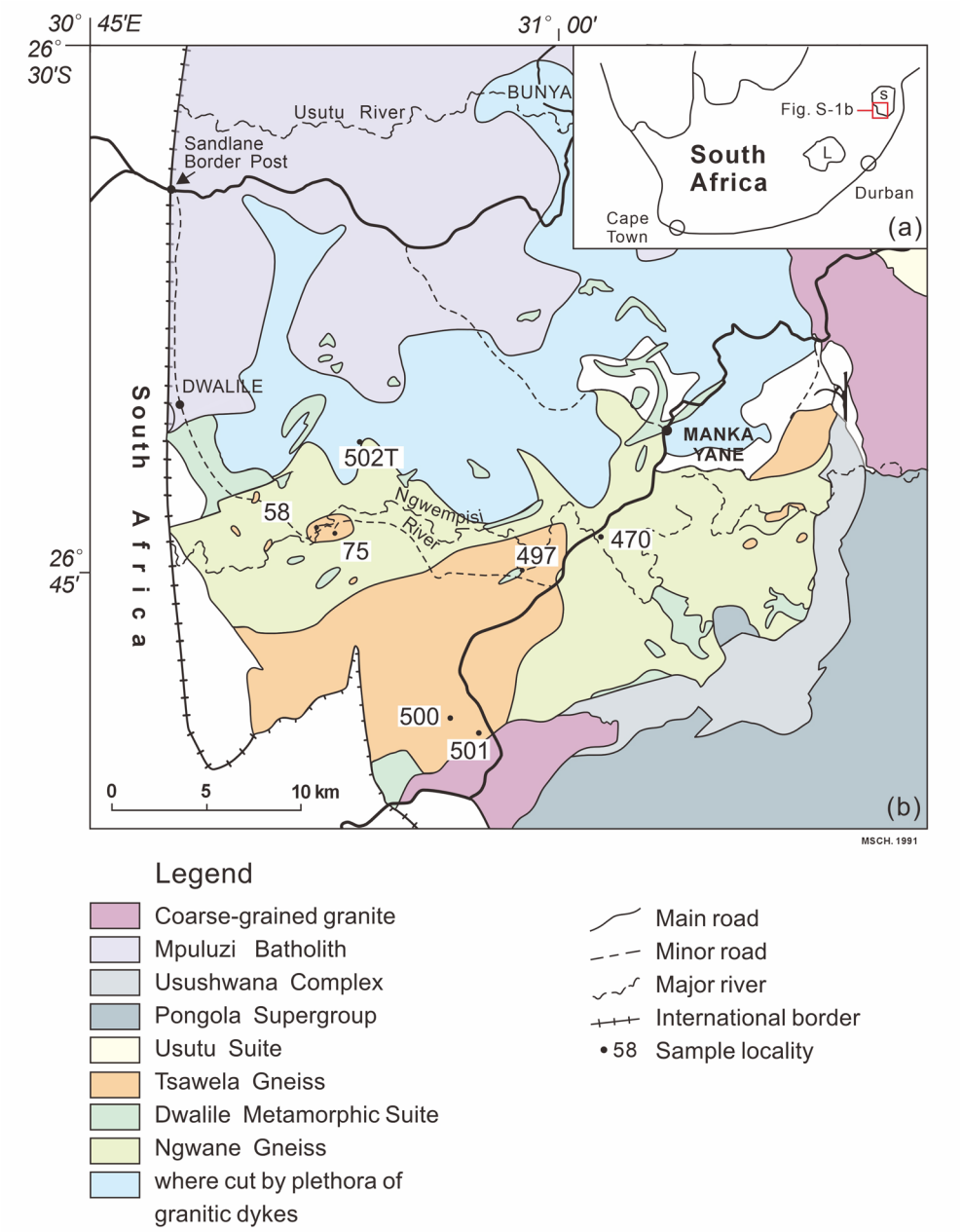

Figure S-1 (a) Simplified geological map of the eastern Kaapvaal Craton. L = Lesotho; S = *Eswatini.* **(b)** Simplified geological map of the Ancient Gneiss Complex (AGC), *Eswatini*, showing the distribution of exposed ~3.45 Ga Ngwane and Tsawela Gneisses and the locations of samples analysed in this study (modified after Hoffmann *et al.*, 2016).

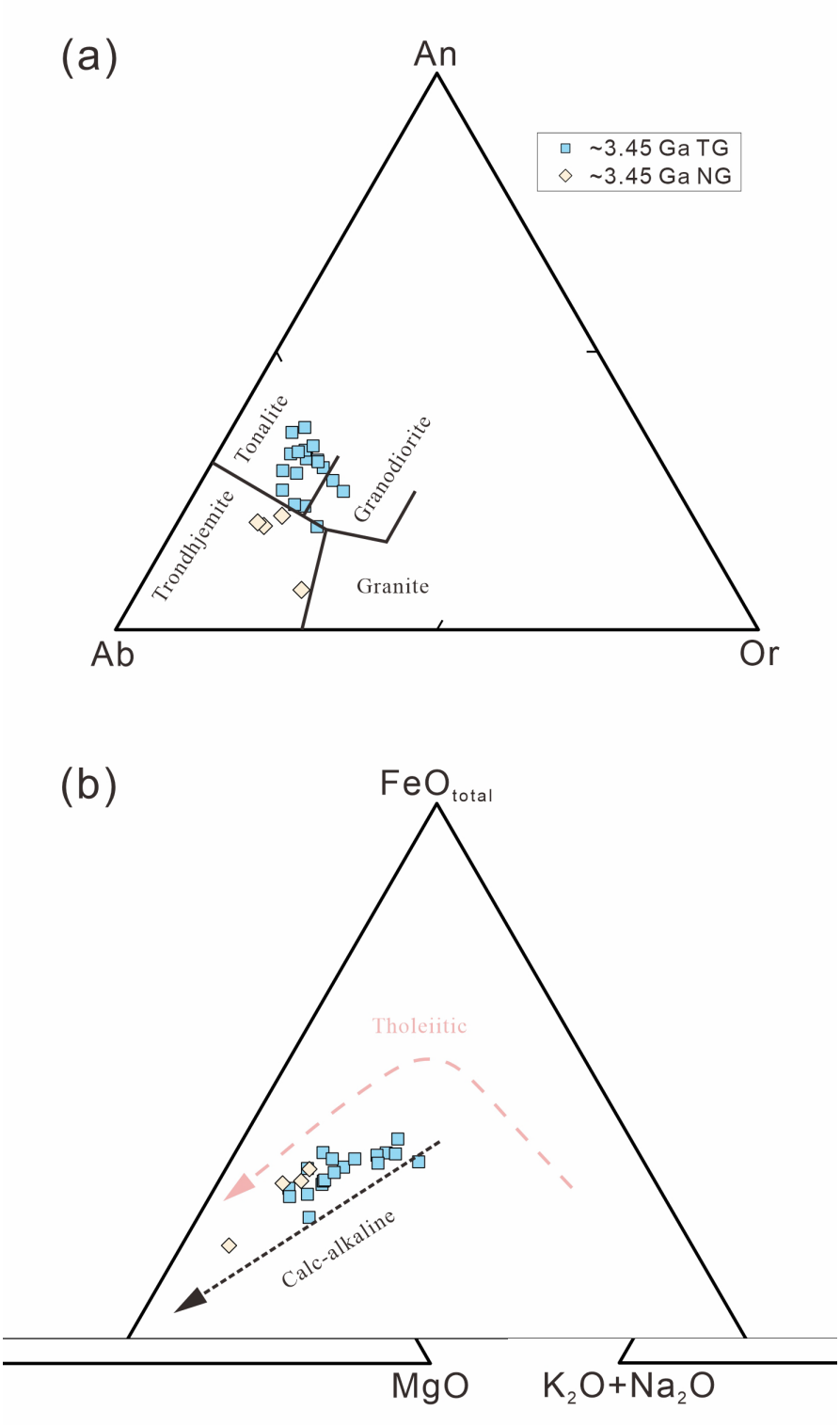

Figure S-2 (a) The Or-An-Ab and **(b)** AFM diagram for ~3.45 Ga TG and NG samples from Irvine and Baragar (1971). All Fe_2O_3 is regarded as FeO_{total}. The data of ~3.45 Ga NG were derived from Hoffmann *et al.* (2016) and Kröner *et al.* (2014).

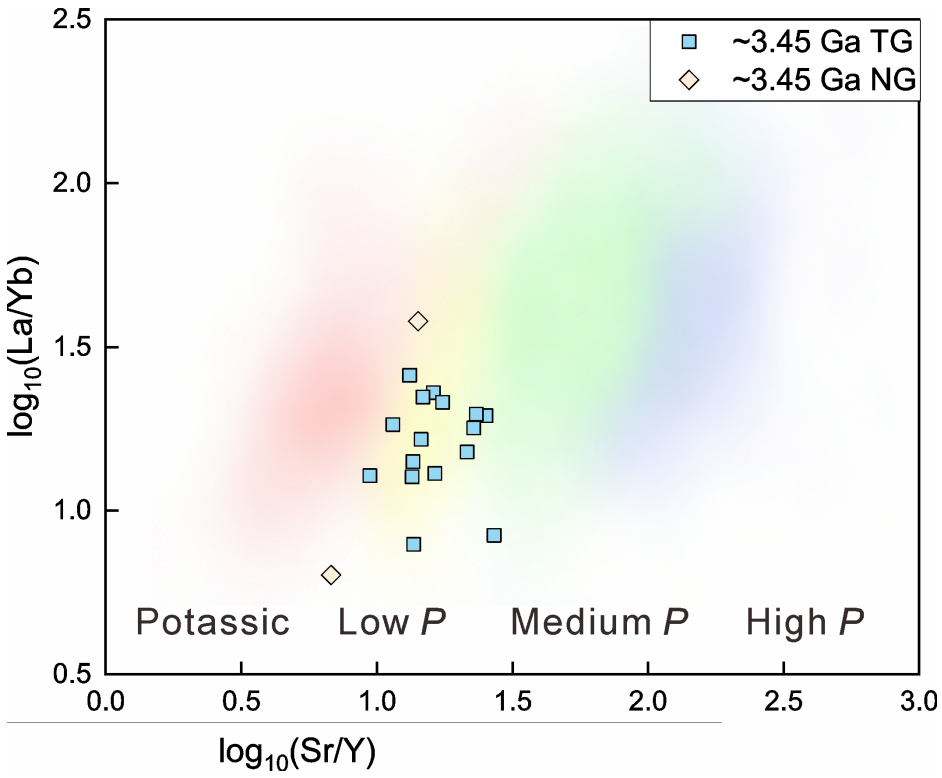

Figure S-3 The $\log_{10}$(Sr/Y) versus $\log_{10}$(La/Yb). The data are derived from Hoffmann *et al.* (2016). The classification background is from Johnson *et al.* (2017).

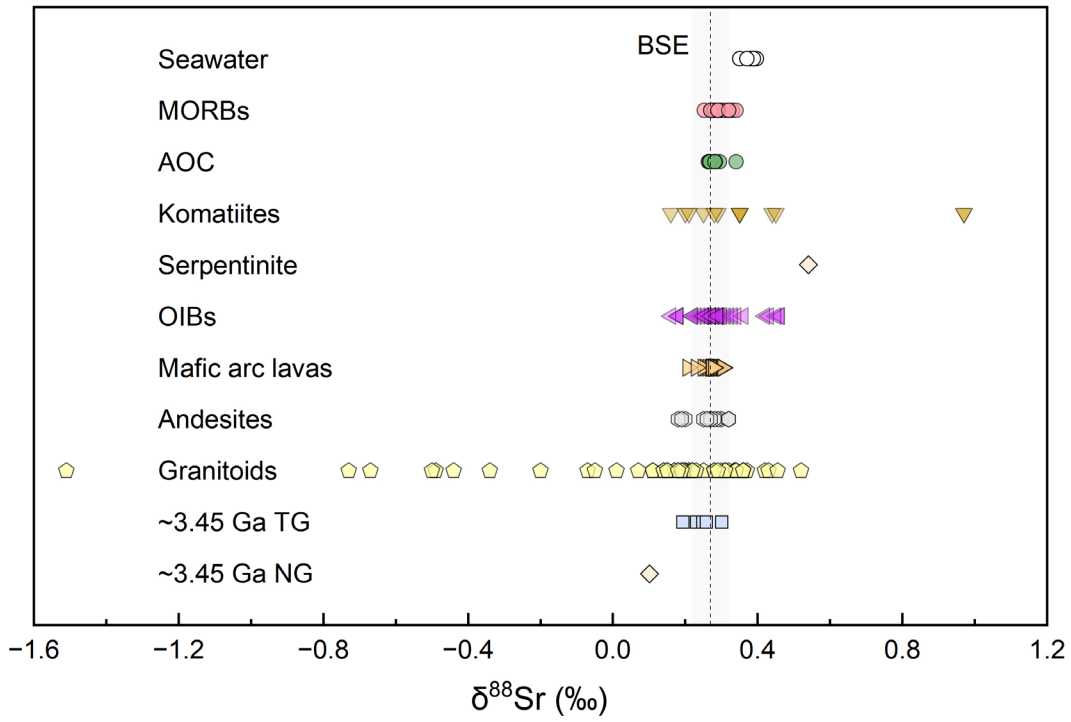

Figure S-4 Stable Sr isotopic compositions of the ~3.45 Ga Tsawela and Ngwane Gneiss (this study), seawater (Liu *et al.*, 2021), MORBs (Charlier *et al.*, 2012; Amsellem *et al.*, 2018; Klaver *et al.*, 2020), altered oceanic crust (AOC) (Klaver *et al.*, 2020), komatiites (Amsellem *et al.*, 2018), serpentinite (Ma *et al.*, 2013), OIBs (Andrews and Jacobson, 2017; Amsellem *et al.*, 2018), mafic arc lavas (Klaver *et al.*, 2020), andesites (Ohno and Hirata, 2007; Moynier *et al.*, 2010; Charlier *et al.*, 2012; Ma *et al.*, 2013; Andrews *et al.*, 2016), and granitoids (Moynier *et al.*, 2010; Charlier *et al.*, 2012; Chen *et al.*, 2025).

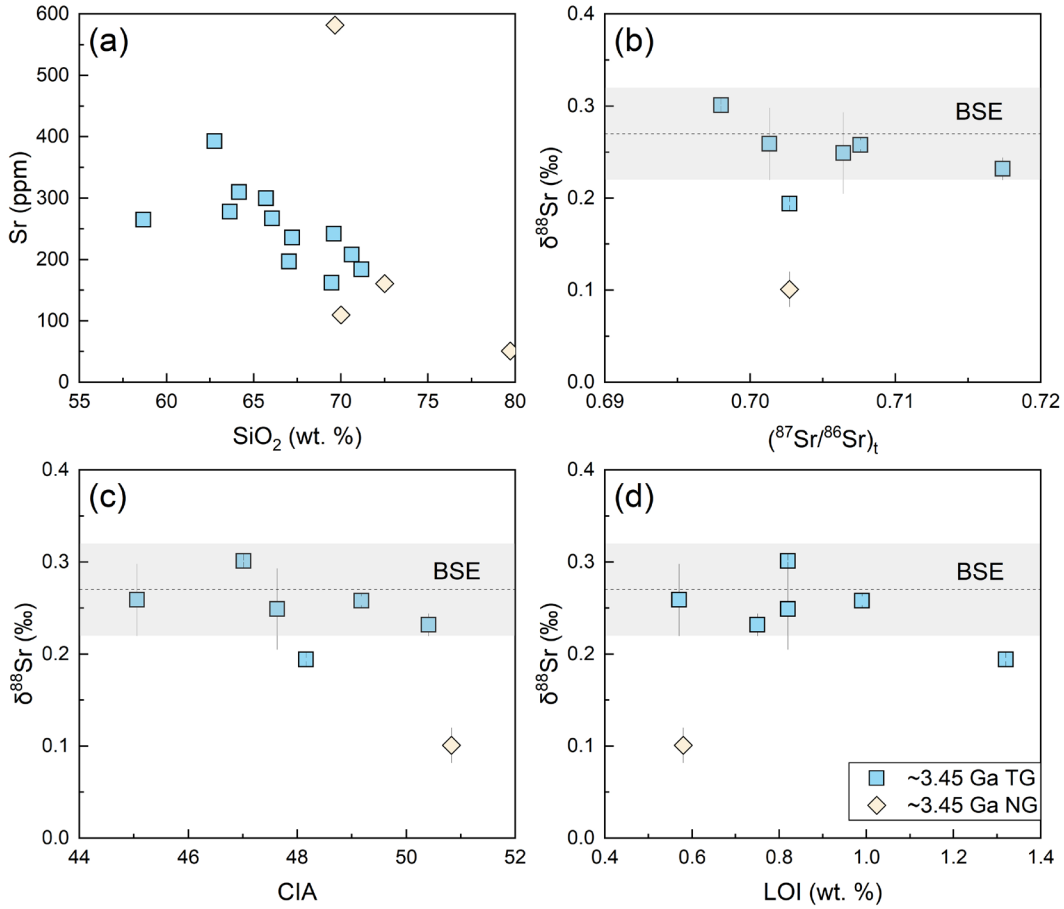

Figure S-5 (a) SiO_2 *vs.* Sr contents; **(b)** $(^{87}Sr/^{86}Sr)_t$ *vs.* $\delta^{88}Sr$, **(c)** $\delta^{88}Sr$ *vs.* LOI, and **(d)** $\delta^{88}Sr$ *vs.* CIA. The BSE value is from Moynier *et al.* (2010).

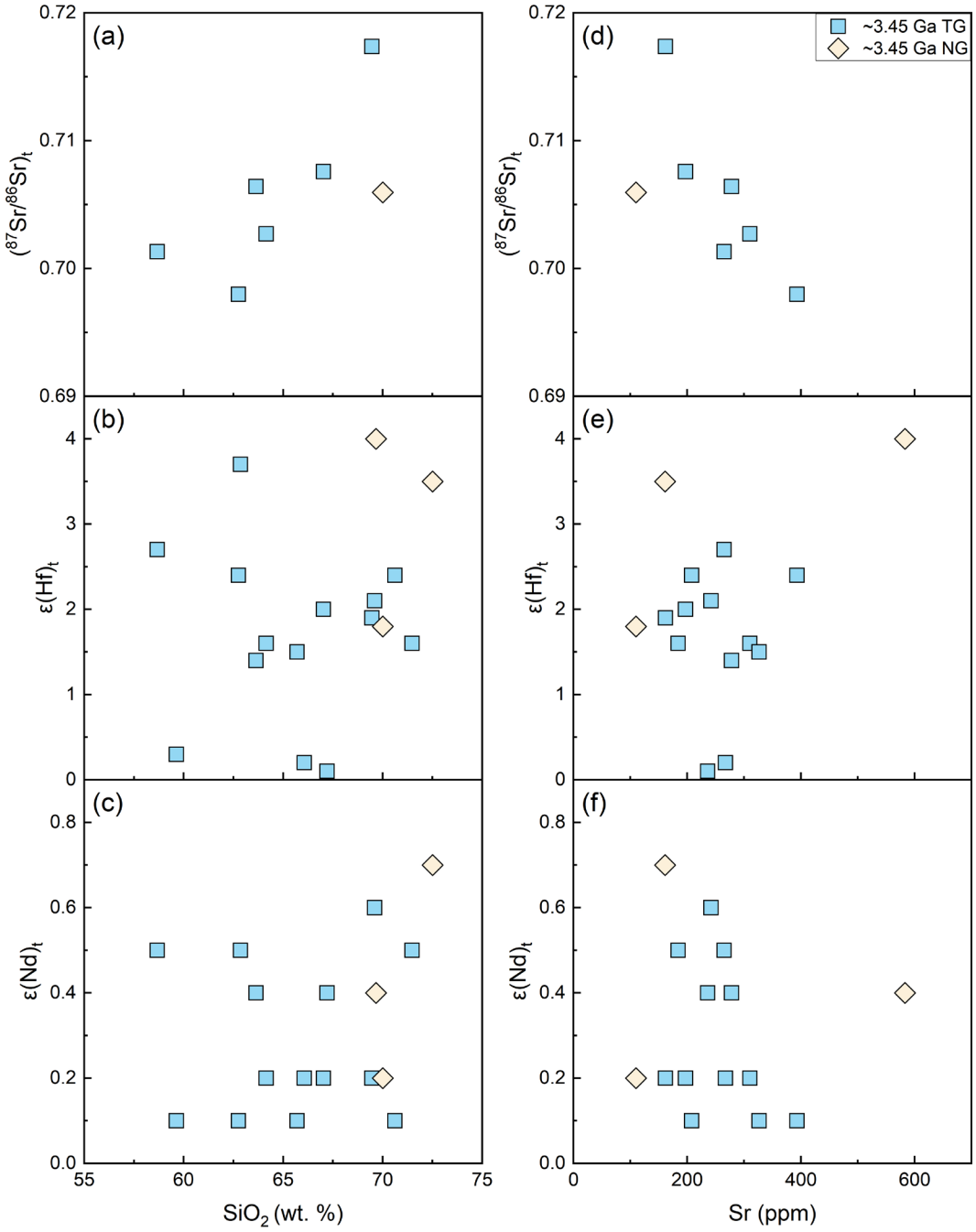

Figure S-6 (a) $(^{87}Sr/^{86}Sr)_t$, **(b)** $\varepsilon(Nd)_t$, and **(c)** $\varepsilon(Hf)_t$ *vs.* SiO_2 and **(d)** $(^{87}Sr/^{86}Sr)_t$, **(e)** $\varepsilon(Nd)_t$, and **(f)** $\varepsilon(Hf)_t$ vs. Sr contents of the TG and NG samples.

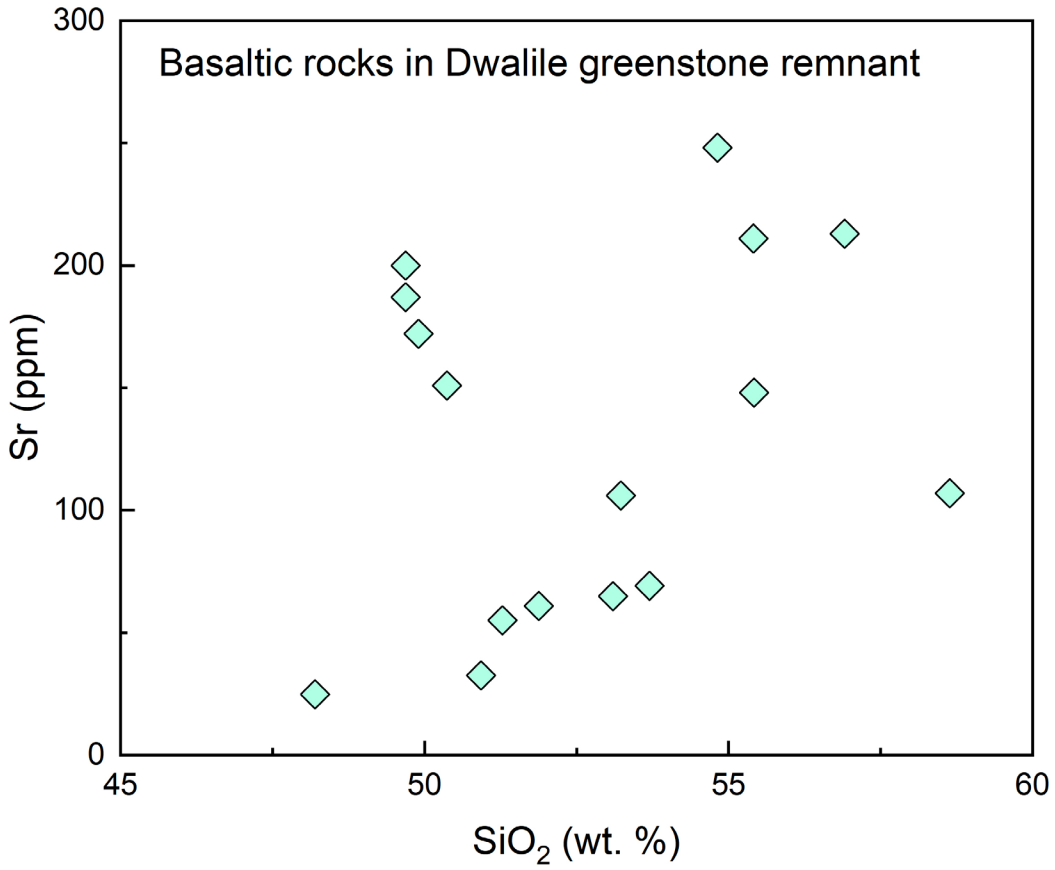

Figure S-7 The SiO_2 vs. Sr content of basaltic rocks in ~3.46 Ga Dwalile greenstone remnants from Hoffmann *et al.* (2020).

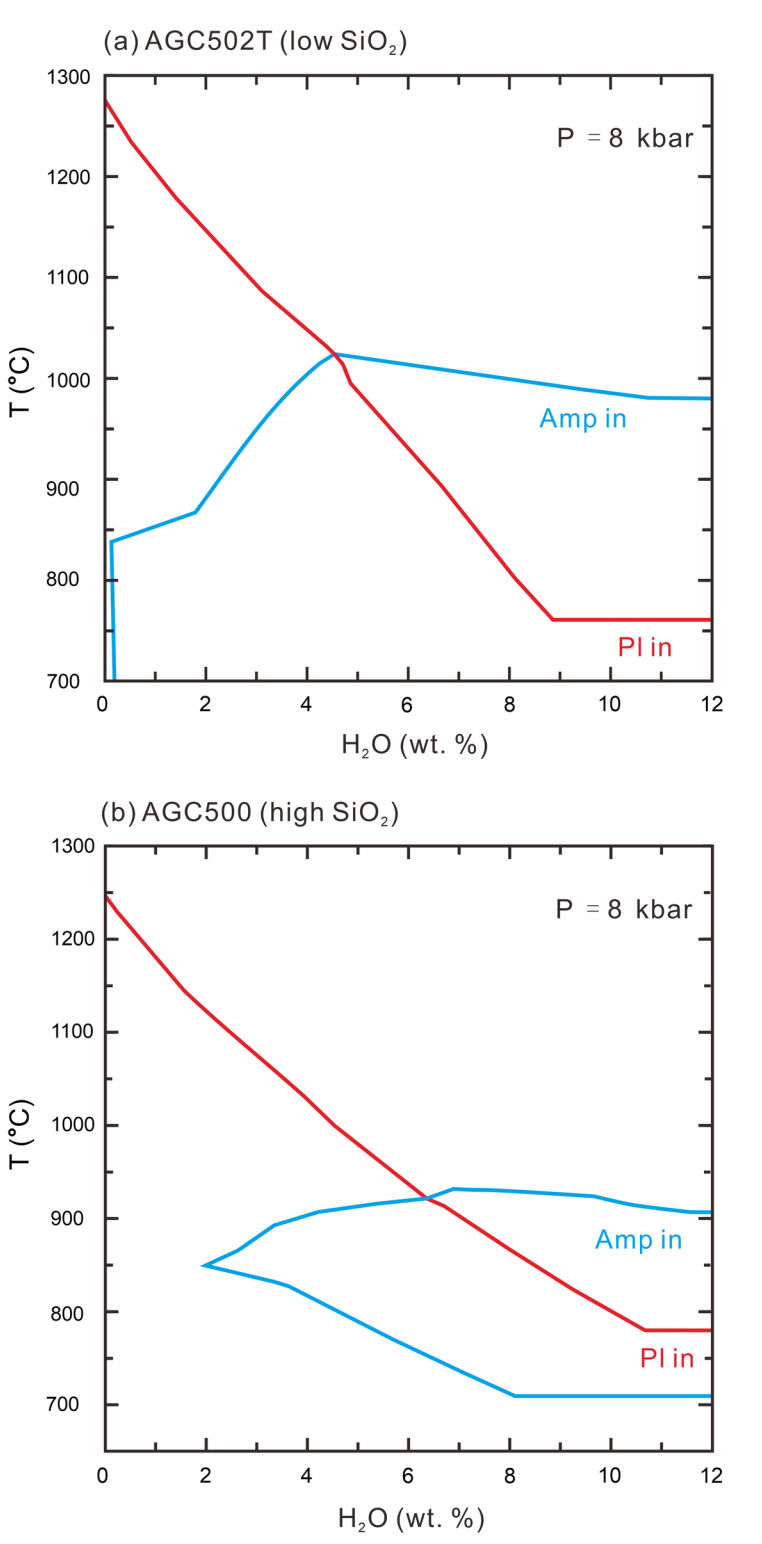

Figure S-8 The T-X(H_2O) pseudosections show the effect of water content on the liquidus temperatures of amphibole (Amp) and plagioclase (Pl) for samples **(a)** AGC502T (low SiO_2) and **(b)** AGC500 (high SiO_2).

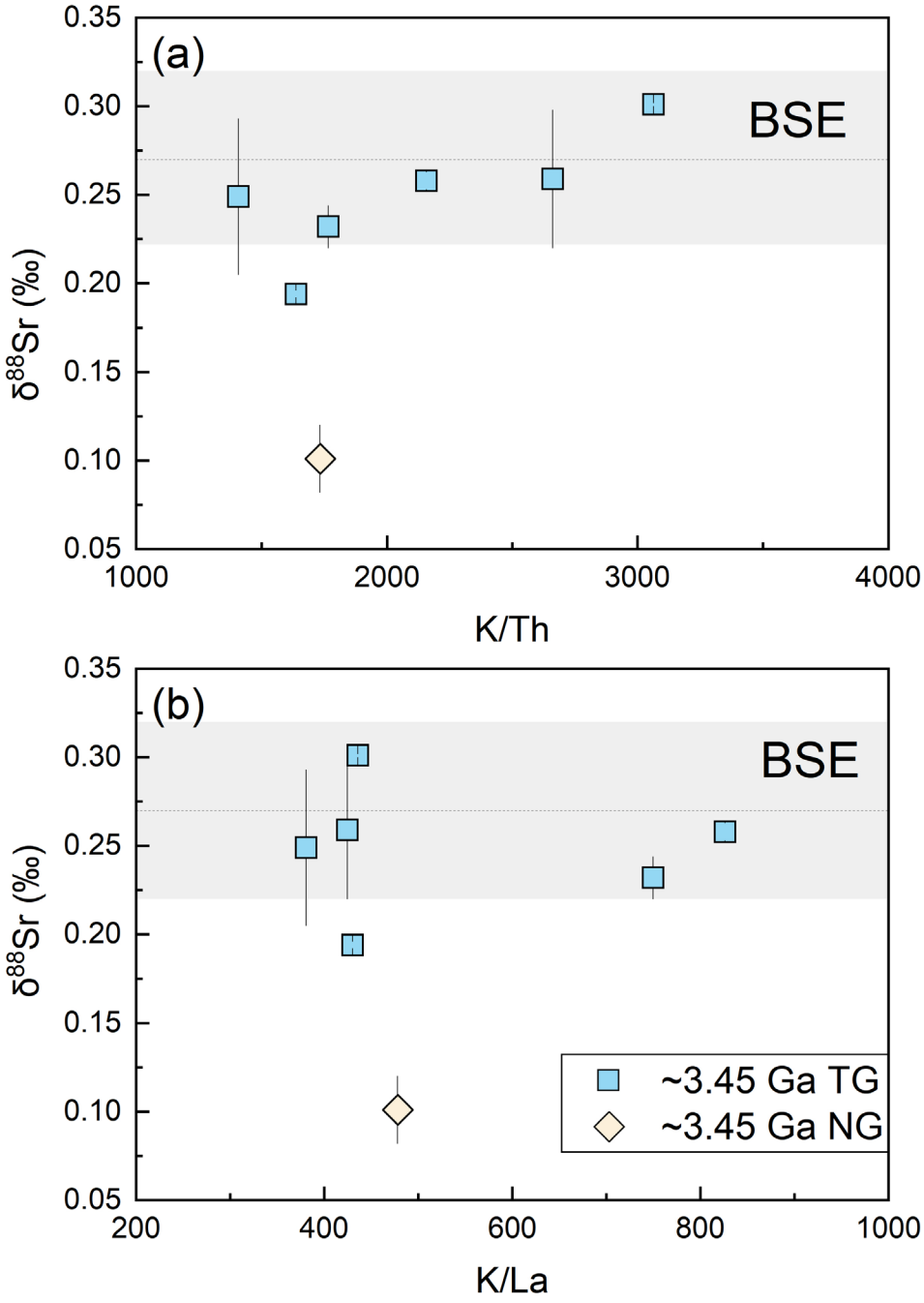

Figure S-9 The $\delta^{88}Sr$ *vs.* **(a)** K/Th and **(b)** K/La ratios of the ~3.45 Ga TG and NG samples.

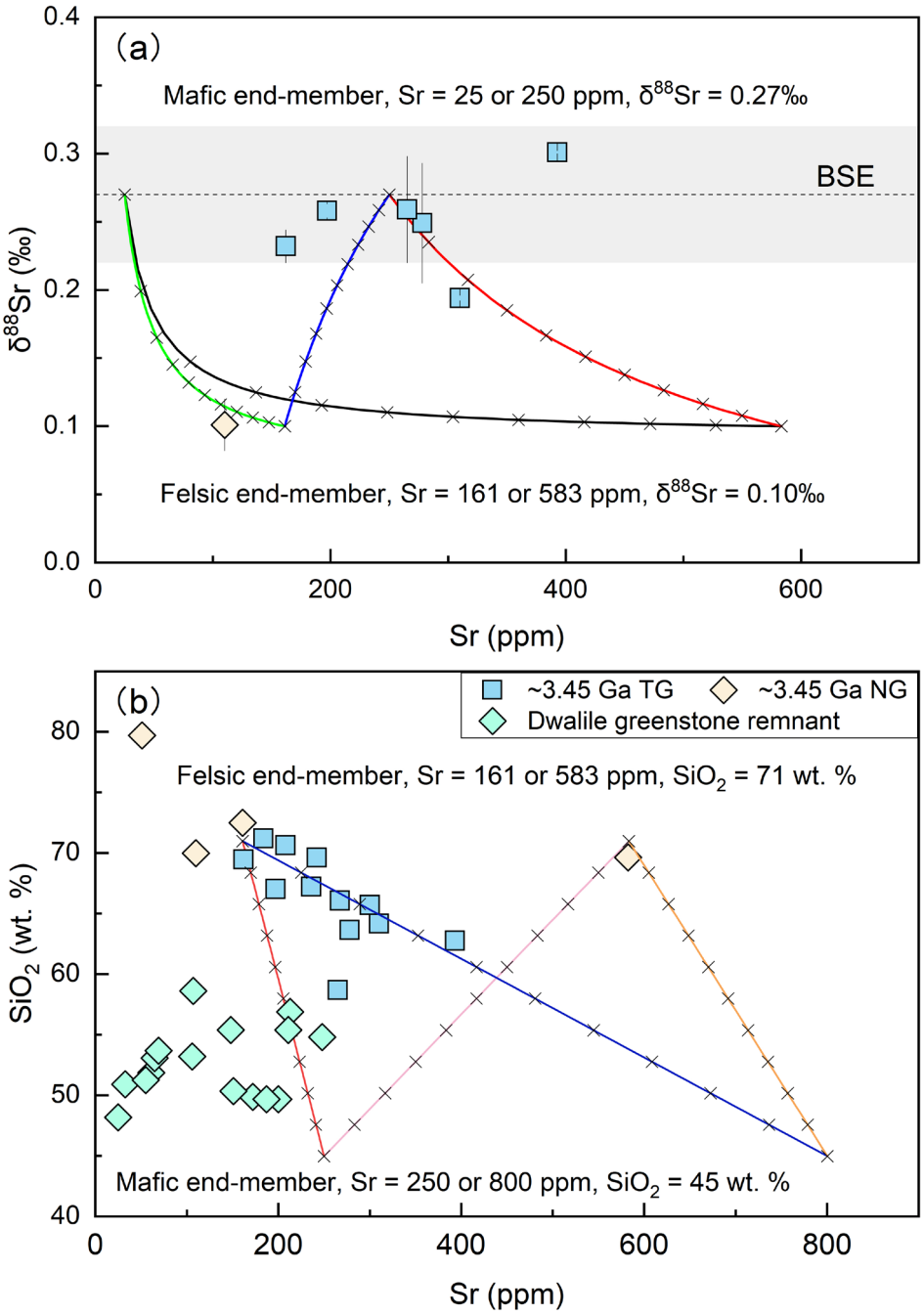

Figure S-10 The binary-mixing modeling of mafic and felsic melts in **(a)** Sr *vs.* $\delta^{88}Sr$ and **(b)** Sr *vs.* SiO_2 space. The cross markers on each curve represent 10 wt. % increments of the mixed melt. The data of ~3.45 Ga NG and TG were derived from Hoffmann *et al.* (2016) and Kröner *et al.* (2014). The compositions of Dwalile greenstone remnants are derived from Hoffmann *et al*. (2020).

Figure S-11 Field photograph of the TG sample AGC 497, showing its fresh appearance and the absence of petrographic evidence for fluid-mediated metasomatism (e.g., quartz veining, epidotisation or partial melt veins).

Table S-1 Stable Sr isotopic compositions of the Tsawela Gneiss and Ngwane gneiss, Ancient Gneiss Complex, Eswatini.

Sample	$^{87}Sr/^{86}Sr$			$\delta^{88}Sr$ (‰)			$^{87}Sr/^{86}Sr$ (Age)	Sr^c (µg/g)	Y^c (µg/g)	Sr/Y^c	Age^c (Ma)	Eu/Eu^{*c}	CIA^d
	Average	2SD[a]	N[b]	Average	2SD	N							
Tsawela gneiss													
AGC58	0.723139	0.000016	2	0.19	0.00	2	0.70271	310	14.4	21.53	3457.8±0.8	0.90	48
AGC75	0.726724	0.000006	2	0.30	0.00	2	0.69799	393	15.5	25.29	3478.1±1.2	0.87	47
AGC497	0.759063	0.000024	2	0.26	0.01	2	0.70759	197	14.5	13.59	3436 (?)	0.83	49
AGC500	0.773669	0.000037	2	0.23	0.01	2	0.71737	162	17.2	9.42	3450 (?)	0.74	50
AGC501	0.733210	0.000030	2	0.27	0.00	2	0.70607	278	19.1	14.55	3441±2.3	0.82	48
Replicate[e]	0.733899	0.000041	2	0.23	0.01	2	0.70676						
Average	0.733555	0.000796	4	0.25	0.04	4	0.70642						
AGC502T	0.723205	0.000006	2	0.28	0.02	2	0.70092	265	16.2	16.36	<3447	0.94	45
Replicate	0.724005	0.000041	2	0.24	0.02	2	0.70172						
Average	0.723605	0.000924	4	0.26	0.04	4	0.70132						
Ngwane gneiss													
AGC470	0.758072	0.000001	2	0.09	0.01	2	0.70596	110	46.7	2.35	3453.3±1.3	0.78	51
Replicate	0.758094	0.000006	2	0.11	0.00	2	0.70598						
Average	0.758083	0.000025	4	0.10	0.02	4	0.70597						
Reference materials													
GBW07104	0.704930	0.000023	2	0.23	0.02	2							
BHVO-2	0.703476	0.000015	2	0.25	0.01	2							
RGM-1	0.704201	0.000012	2	0.18	0.03	2							

[a] 2SD represents twice the standard deviation of the population of N repeated measurements of the same sample. [b] N indicates the number of mass

spectrometry analyses for the same sample.[c] data derived from Hoffmann *et al*. (2016), $Eu/Eu^{*}=Eu_N/\sqrt{(Sm_N \times Gd_N)}$, where subscript N denotes CI chondrite-normalised values from Sun and McDonough (1989).[d] $CIA = [Al_2O_3/(Al_2O_3+CaO^{*}+Na_2O+K_2O)]*100$, the chemical index of alteration (CIA) using molecular proportions, CaO^{*} is the amount of CaO in the silicate fraction of the rock (Nesbitt and Young, 1982). [e] Replicate implies repeated sample dissolution, column chemistry and analysis.

Table S-2 The bulk-rock compositions (wt. %) for phase-equilibrium modeling.

Sample	AGC502T					AGC500				
SiO_2	58.92	57.72	55.31	60.12	52.90	69.56	68.14	65.30	70.98	62.46
TiO_2	0.63	0.61	0.59	0.64	0.56	0.38	0.37	0.36	0.39	0.34
Al_2O_3	17.04	16.69	16.00	17.39	15.30	14.45	14.16	13.57	14.75	12.98
FeO	5.38	5.27	5.05	5.49	4.83	3.11	3.04	2.92	3.17	2.79
MnO	0.09	0.09	0.08	0.09	0.08	0.06	0.06	0.06	0.06	0.05
MgO	3.59	3.52	3.37	3.67	3.23	1.29	1.27	1.21	1.32	1.16
CaO	6.85	6.71	6.43	6.99	6.15	3.07	3.00	2.88	3.13	2.75
Na_2O	4.34	4.25	4.07	4.43	3.90	3.71	3.64	3.49	3.79	3.33
K_2O	1.11	1.08	1.04	1.13	0.99	2.34	2.29	2.20	2.39	2.10
O_2	0.06	0.06	0.06	0.06	0.06	0.03	0.03	0.03	0.03	0.03
H_2O	2.00	4.00	8.00	0.00	12.00	2.00	4.00	8.00	0.00	12.00
Total	100	100	100	100	100	100	100	100	100	100
Figure	3a	3a	3a	S-8a	S-8a	3b	3b	3b	S-8b	S-8b

Note: H_2O was varied systematically to evaluate its effect on the plagioclase and amphibole liquidus temperatures, while the relative proportions of other major-element components were kept constant and the compositions were renormalized to 100 wt. %.

References

Amsellem, E., Moynier, F., Day, J.M.D., Moreira, M., Puchtel, I.S., Teng, F.Z. (2018) The stable strontium isotopic composition of ocean island basalts, mid-ocean ridge basalts, and komatiites. *Chemical Geology* 483, 595-602. https://doi.org/10.1016/j.chemgeo.2018.03.030

Andrews, M.G., Jacobson, A.D. (2017) The radiogenic and stable Sr isotope geochemistry of basalt weathering in Iceland: Role of hydrothermal calcite and implications for long-term climate regulation. *Geochimica et Cosmochimica Acta* 215, 247-262. https://doi.org/10.1016/j.gca.2017.08.012

Andrews, M.G., Jacobson, A.D. (2018) Controls on the solute geochemistry of subglacial discharge from the Russell Glacier, Greenland Ice Sheet determined by radiogenic and stable Sr isotope ratios. *Geochimica et Cosmochimica Acta* 239, 312-329. https://doi.org/10.1016/j.gca.2018.08.004

Andrews, M.G., Jacobson, A.D., Lehn, G.O., Horton, T.W., Craw, D. (2016) Radiogenic and stable Sr isotope ratios ($^{87}Sr/^{86}Sr$, $\delta^{88/86}Sr$) as tracers of riverine cation sources and biogeochemical cycling in the Milford Sound region of Fiordland, New Zealand. *Geochimica et Cosmochimica Acta* 173, 284-303. https://doi.org/10.1016/j.gca.2015.10.005

Beard, J.S., Lofgren, G.E. (1991) Dehydration Melting and Water-Saturated Melting of Basaltic and Andesitic Greenstones and Amphibolites at 1, 3, and 6. 9 kb. *Journal of Petrology* 32, 365-401. https://doi.org/10.1093/petrology/32.2.365

Caton, S.A., Smit, M.A., Emo, R.B., Musiyachenko, K.A., Kielman-Schmitt, M., Kooijman, E., Scherstén, A., Halla, J., Bleeker, W., Hoffmann, J.E., Pandey, O.P., Ravindran, A., Maltese, A., Mezger, K. (2022) Evolution of the sources of TTG and associated rocks during the Archean from in-situ $^{87}Sr/^{86}Sr$ isotope analysis of apatite by LA-MC-ICPMS. *Lithos* 428-429, 106830. https://doi.org/10.1016/j.lithos.2022.106830

Charlier, B.L.A., Nowell, G.M., Parkinson, I.J., Kelley, S.P., Pearson, D.G., Burton, K.W. (2012) High temperature strontium stable isotope behaviour in the early solar system and planetary bodies. *Earth and Planetary Science Letters* 329-330, 31-40. https://doi.org/10.1016/j.epsl.2012.02.008

Chen, X.Q., Deng, G.X., Jiang, D.S., Nan, X.Y., Huang, F. (2025) Stable strontium isotope fractionation during crystal-melt separation in granitic magma evolution. *Acta Geochimica* 44, 731-739. https://doi.org/10.1007/s11631-024-00752-9

Connolly, J.A.D. (2005) Computation of phase equilibria by linear programming: A tool for geodynamic modeling and its application to subduction zone decarbonation. *Earth and Planetary Science Letters* 236, 524-541. https://doi.org/10.1016/j.epsl.2005.04.033

Davies, R.D., Allsopp, H.L. (1976) Strontium isotopic evidence relating to the evolution of the lower Precambrian granitic crust in Swaziland. *Geology* 4, 553-556. https://doi.org/10.1130/0091-7613(1976)4<553:SIERTT>2.0.CO;2

Green, E.C.R., White, R.W., Diener, J.F.A., Powell, R., Holland, T.J.B., Palin, R.M. (2016) Activity-composition relations for the calculation of partial melting equilibria in metabasic rocks. *Journal of Metamorphic Geology* 34, 845-869. https://doi.org/10.1111/jmg.12211

Hanson, G.N. (1978) The application of trace elements to the petrogenesis of igneous rocks of granitic composition. *Earth and Planetary Science Letters* 38, 26-43. https://doi.org/10.1016/0012-821X(78)90124-3

Hoffmann, J.E., Kröner, A., Hegner, E., Viehmann, S., Xie, H., Iaccheri, L.M., Schneider, K.P., Hofmann, A., Wong, J., Geng, H., Yang, J. (2016) Source composition, fractional crystallization and magma mixing processes in the 3.48–3.43Ga Tsawela tonalite suite (Ancient Gneiss Complex, Swaziland) – Implications for Palaeoarchaean geodynamics. *Precambrian Research* 276, 43-66. https://doi.org/10.1016/j.precamres.2016.01.026

Hoffmann, J.E., Musese, E., Kröner, A., Schneider, K.P., Wong, J., Hofmann, A., Hegner, E., Kasper, H.U., Tusch, J., Münker, C. (2020) Hafnium-Neodymium isotope, trace element and U-Pb zircon age constraints on the petrogenesis of the 3.44–3.46 Ga Dwalile greenstone remnant, Ancient gneiss Complex, Swaziland. *Precambrian Research* 351, 105970. https://doi.org/10.1016/j.precamres.2020.105970

Holland, T., Powell, R. (2003) Activity–composition relations for phases in petrological calculations: an asymmetric multicomponent formulation. *Contributions to Mineralogy and Petrology* 145, 492-501. https://doi.org/10.1007/s00410-003-0464-z

Holland, T.J.B., Powell, R. (2011) An improved and extended internally consistent thermodynamic dataset for phases of petrological interest, involving a new equation of state for solids. *Journal of Metamorphic Geology* 29, 333-383. https://doi.org/10.1111/j.1525-1314.2010.00923.x

Irvine, T.N., Baragar, W.R.A. (1971) A Guide to the Chemical Classification of the Common Volcanic Rocks. *Canadian Journal of Earth Sciences* 8, 523-548. https://doi.org/10.1139/e71-055

Johnson, T.E., Brown, M., Gardiner, N.J., Kirkland, C.L., Smithies, R.H. (2017) Earth's first stable continents did not form by subduction. *Nature* 543, 239-242. https://doi.org/10.1038/nature21383

Klaver, M., Lewis, J., Parkinson, I.J., Elburg, M.A., Vroon, P.Z., Kelley, K.A., Elliott, T. (2020) Sr isotopes in arcs revisited: tracking slab dehydration using $\delta^{88/86}Sr$ and $^{87}Sr/^{86}Sr$ systematics of arc lavas. *Geochimica et Cosmochimica Acta* 288, 101-119. https://doi.org/10.1016/j.gca.2020.08.010

Kröner, A., Hoffmann, J.E., Xie, H., Münker, C., Hegner, E., Wan, Y., Hofmann, A., Liu, D., Yang, J. (2014) Generation of early Archaean grey gneisses through melting of older crust in the eastern Kaapvaal craton, southern Africa.

Precambrian Research 255, 823-846. https://doi.org/10.1016/j.precamres.2014.07.017

Liu, H.C., Chen, Y.H., You, C.F., Chung, C.H. (2021) Precise $\delta^{88/86}$Sr determination on a MC-ICP-MS by an improved method combining Zr-empirical external normalization isobaric interference correction and ^{84}Sr-^{87}Sr double spike. *Journal of Analytical Atomic Spectrometry* 36, 2322-2329. https://doi.org/10.1039/d1ja00224d

Luo, K., Ma, J., Wang, Z., Zhu, G., Zeng, T., Wei, G. (2024) Fractionation Mechanism and Flux Estimation of Strontium Isotopes During Basalt Weathering. *Geochemistry, Geophysics, Geosystems* 25, e2023GC011215. https://doi.org/10.1029/2023GC011215

Ma, J.L., Wei, G.J., Liu, Y., Ren, Z.Y., Xu, Y.G., Yang, Y.H. (2013) Precise measurement of stable ($\delta^{88/86}$Sr) and radiogenic (^{87}Sr/^{86}Sr) strontium isotope ratios in geological standard reference materials using MC-ICP-MS. *Chinese Science Bulletin* 58, 3111-3118. https://doi.org/10.1007/s11434-013-5803-5

Moynier, F., Agranier, A., Hezel, D.C., Bouvier, A. (2010) Sr stable isotope composition of Earth, the Moon, Mars, Vesta and meteorites. *Earth and Planetary Science Letters* 300, 359-366. https://doi.org/10.1016/j.epsl.2010.10.017

Müntener, O., Ulmer, P. (2018) Arc crust formation and differentiation constrained by experimental petrology. *American Journal of Science* 318, 64-89. https://doi.org/10.2475/01.2018.04

Nandedkar, R.H., Ulmer, P., Müntener, O. (2014) Fractional crystallization of primitive, hydrous arc magmas: an experimental study at 0.7 GPa. *Contributions to Mineralogy and Petrology* 167, 1015. https://doi.org/10.1007/s00410-014-1015-5

Nesbitt, H., Young, G. (1982) Early Proterozoic climates and plate motions inferred from major element chemistry of lutites. *Nature* 299, 715-717. https://doi.org/10.1038/299715a0

Ohno, T., Hirata, T. (2007) Simultaneous Determination of Mass-dependent Isotopic Fractionation and Radiogenic Isotope Variation of Strontium in Geochemical Samples by Multiple Collector-ICP-Mass Spectrometry. *Analytical Sciences* 23, 1275-1280. https://doi.org/10.2116/analsci.23.1275

Pichavant, M., Macdonald, R. (2007) Crystallization of primitive basaltic magmas at crustal pressures and genesis of the calc-alkaline igneous suite: experimental evidence from St Vincent, Lesser Antilles arc. *Contributions to Mineralogy and Petrology* 154, 535-558. https://doi.org/10.1007/s00410-007-0208-6

Sun, S.S., McDonough, W.F. (1989) Chemical and isotopic systematics of oceanic basalts: Implications for mantle composition and processes. *Geological Society London Special Publications* 42, 313-345. https://doi.org/10.1144/GSL.SP.1989.042.01.19

Thy, P., Lofgren, G.E. (1994) Experimental constraints on the low-pressure evolution of transitional and mildly alkalic basalts: the effect of Fe-Ti oxide minerals and the origin of basaltic andesites. *Contributions to Mineralogy and Petrology* 116, 340-351. https://doi.org/10.1007/BF00306502

White, R.W., Powell, R., Holland, T.J.B., Johnson, T.E., Green, E.C.R. (2014) New mineral activity–composition relations for thermodynamic calculations in metapelitic systems. *Journal of Metamorphic Geology* 32, 261-286. https://doi.org/10.1111/jmg.12071

White, R.W., Powell, R., Holland, T.J.B., Worley, B.A. (2000) The effect of TiO_2 and Fe_2O_3 on metapelitic assemblages at greenschist and amphibolite facies conditions: mineral equilibria calculations in the system K_2O-FeO-MgO-Al_2O_3-SiO_2-H_2O-TiO_2-Fe_2O_3. *Journal of Metamorphic Geology* 18, 497-511. https://doi.org/10.1046/j.1525-1314.2000.00269.x

Zhang, Y., Namur, O., Charlier, B. (2023) Experimental study of high-Ti and low-Ti basalts: liquid lines of descent and silicate liquid immiscibility in large igneous provinces. *Contributions to Mineralogy and Petrology* 178, 7. https://doi.org/10.1007/s00410-022-01990-x